RESEARCH ARTICLE

NANO · MICRO small
www.small-journal.com

Composition Dependent Dynamic Behaviors of Non-Stoichiometric Cocrystalline Hydrogen-Bonded Organic Frameworks

*Taito Hashimoto, Ryusei Oketani, and Ichiro Hisaki**

Non-stoichiometric multicomponent crystals have the potential not only to fine-tune material properties but also to emerge new functionalities. In this paper, the composition-dependent dynamic transformation of non-stoichiometric cocrystalline hydrogen-bonded organic frameworks (NS-HOFs) composed of tetrakis(4-carboxyphenyl)hexahydropyrene and -pyrene derivatives (CP-Hp and CP-Py, respectively) is reported. Isostructural mono-component frameworks of CP-Hp and CP-Py (CP-Hp-1 and CP-Py-1, respectively) underwent structural transformation into the corresponding shrunk frameworks (CP-Hp-2 and CP-Py-2, respectively) by spontaneous release of the included solvent molecules, where the transformation speed of CP-Hp-1 is faster than that of CP-Py-1. NS-HOFs of CP-Hp and CP-Py, denoted by CP-HpPy-1(*x*), where *x* is the mixing ratio of CP-Hp, show the transformation into CP-HpPy-2(*x*), and the transformation behaviors strongly depend on the composition ratio. Interestingly, the transformation speed is not proportional to the composition ratio, while the maximum speed is observed for CP-HpPy-1(0.5). This is, to the best of these knowledge, the first example of composition-dependent structural changes in non-stoichiometric cocrystalline frameworks, demonstrating that dynamic behaviors can be modulated nonlinearly by the composition of the frameworks and shedding light on new aspects of porous soft crystals.

1. Introduction

Non-stoichiometrically mixed multicomponent frameworks make it possible to fine-tune the crystal structures and material properties, and furthermore, to emerge new functionalities which are not achieved by mono-component frameworks.[1–3] These frameworks are of great interest for improving the designability and developing the functionality of organic porous materials. As a pioneering work, in 2010, Yaghi and co-workers prepared multicomponent metal-organic frameworks (MOFs)[4–6] using several *para*-phenylene ligands with different functional groups and demonstrated that multicomponent MOFs exhibit high selective uptake of CO_2 over CO compared with pristine MOF-5.[7] In the case of covalent-organic frameworks (COF),[8–10] Dichtel and co-workers constructed 2D COFs using triaminophenylbenzene and two different dicarboxyphenyl derivatives, showing the possibility of synthesizing structurally and functionally complex COFs depending on the composition ratio.[11] MOFs and COFs are becoming a sophisticated platform to study non-stoichiometric multicomponent frameworks because strong metal coordination bonds and covalent bonds make it easy to mix multicomponents into the frameworks. Thus far, a lot of examples have been reported to tune or improve their material properties, such as absorption selectivity,[12] emission property,[13–15] catalytic activity,[16] and electronic property.[17,18]

On the other hand, it has been generally difficult to construct non-stoichiometric cocrystalline hydrogen-bonded organic frameworks (NS-HOFs), where an HOF[19–21] is a crystalline porous framework constructed by self-assembling molecules through hydrogen bonds (H-bonds). This is because H-bonding formation is highly reversible, and therefore, thermodynamically more stable frameworks tend to form. To date, only a few examples of NS-HOFs have been reported.[22–26] We have demonstrated that tetracarboxylic acid derivatives based on pyrene and hydropyrene skeletons (**CP-Py** and **CP-Hp**, respectively) yielded single crystals of NS-HOFs named **CP-HpPy-1**,[24] where **CP-Py** and **CP-Hp** are contained with a non-stoichiometric ratio in the framework, and their composition of each single crystal is capable of being determined from single crystal X-ray diffraction (SCXRD) analysis. Since HOFs usually exhibit high crystallinity and the single crystals suitable for SCXRD analysis are easily obtained, it is possible to conduct the precise structural analysis of

T. Hashimoto, R. Oketani, I. Hisaki
Division of Chemistry
Graduate School of Engineering Science
The University of Osaka
1-3 Machikaneyama, Toyonaka, Osaka 560–8531, Japan
E-mail: i.hisaki.es@osaka-u.ac.jp

The ORCID identification number(s) for the author(s) of this article can be found under https://doi.org/10.1002/smll.202508763

DOI: 10.1002/smll.202508763

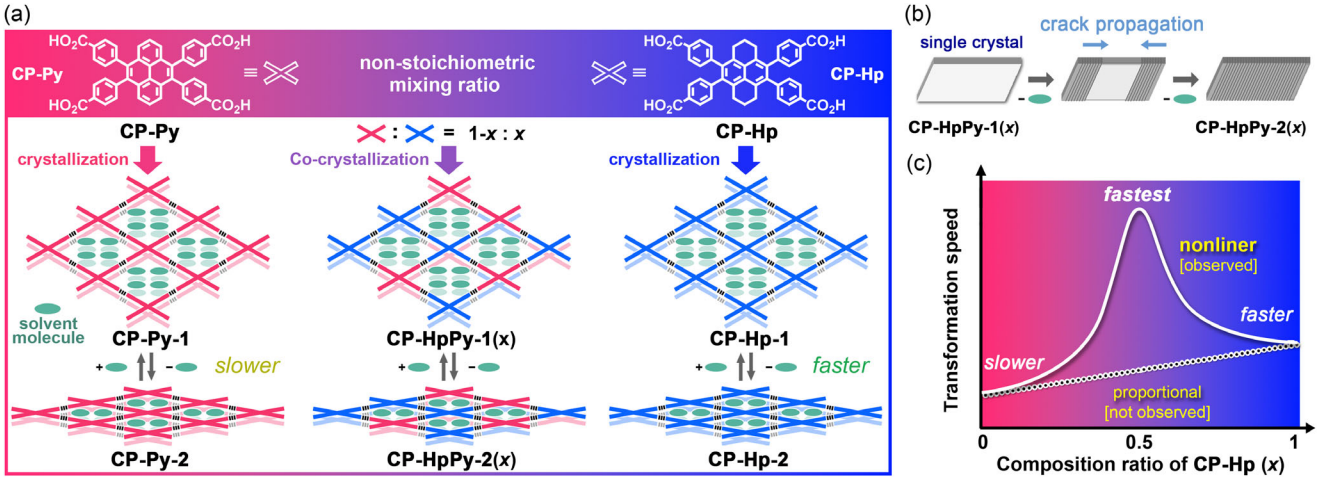

Figure 1. Composition-dependent structural transformation of non-stoichiometric hydrogen-bonded organic frameworks (NS-HOFs). a) Schematic representation for structural transformation of NS-HOFs **CP-HpPy-1**(*x*) into **CP-HpPy-2**(*x*) with shrunk apertures by spontaneous solvent release. The NS-HOFs are composed of hydropyrene and pyrene derivatives (**CP-Hp** and **CP-Py**, respectively) with a mixing ratio of *x*: 1−*x*. b) Cracking in a single crystal of the framework upon the structural transformation. c) Schematic diagram for the transformation speed of **CP-Hp-1**, **CP-Py-1**, and **CP-HpPy-1**(*x*). The speed of **CP-Hp-1** is larger than that of **CP-Py-1**, while the speed of **CP-HpPy-1**(*x*) changes in a nonlinear manner depending on the composition ratio of **CP-Hp** and **CP-Py**. **CP-HpPy-1**(0.5) exhibits the maximum transformation speed.

the non-stoichiometric framework, which is difficult with MOFs and COFs due to structural defects. More recently, tuning the material properties has been achieved with the NS-HOF system. Chen and co-workers prepared NS-HOFs with permanent porosity using pyrene-based derivatives bearing —H, —CH_3, —NH_2, and —F groups and demonstrated that hydrophobicity can be modulated depending on the component fraction.[25] Our groups constructed the NS-HOF $\mathbf{B_TN_T}$**-1** using two tetracarboxylic acid derivatives with benzothiazole and naphthalene moieties (**BTTA** and **NTTA**, respectively) and demonstrated that versatile fluorescent colors can be achieved on the single crystal of NS-HOF depending on the composition ratio and distribution manner of the components in the crystal.[26]

During our study on NS-HOF **CP-HpPy-1**, we found that mono-component HOF **CP-Py-1** undergoes reversible structural transformation with shrinkage and expansion of the voids upon desorption and adsorption of guest molecules, which was confirmed by SCXRD analysis of both structures.[27] Molecule-based flexible frameworks have been gaining attention as new functional porous materials from the viewpoint that they can change their crystal structures in response to external stimuli.[28–31] Although HOFs capable of changing their crystal structures triggered by the guest molecules are also reported,[32–41] tuning of their dynamic behaviors has been unexplored. In connection with this, the flexible nature of **CP-Py-1** inspired us to modulate the structural transformation behavior of NS-HOFs by changing the composition ratio in a single crystal.

Herein, we demonstrate composition-dependent dynamic structural transformation of NS-HOFs, whose structures are well-characterized by SCXRD analysis. The transformation of NS-HOF **CP-HpPy-1** was reversibly induced by desorption and adsorption of aromatic guest molecules (**Figure 1a**), accompanied by propagation of cracks in the single crystal (Figure 1b). **CP-HpPy-1** transforms into either of the two crystalline forms depending on the major components in the crystal. Furthermore, it is remarkable that the transformation speed nonlinearly depends on the composition ratio of the NS-HOF: the maximum speed was achieved in the case of the ratio of 0.5:0.5 (Figure 1c). This is the first example of the composition-dependent structural transformation of the non-stoichiometric frameworks, shedding light on a new aspect of multicomponent porous materials.

2. Results and Discussion

2.1. Structural Transformation of Monocomponent HOF CP-Hp-1

Mono-component HOFs **CP-Py-1** and **CP-Hp-1** were prepared by slow evaporation of their solutions dissolved in *N*,*N*-dimethylformamide (DMF) and 1,2-dichlorobenzene (DCB) at 60 °C according to our previous report,[24] giving single crystals of HOFs **CP-Py-1** and **CP-Hp-1**, respectively. These HOFs have nearly the same structures as each other (Figure S1, Supporting Information): molecules are connected through H-bonding between the carboxy groups to form a 2D ***sql***-topological network layer, and the layers are slip-stacked to give the HOFs. Structural change of **CP-Py-1**, which has been reported before,[27] was summarized in Figure S2 (Supporting Information). As shown in **Figure 2a,b**, we found that **CP-Hp-1** also underwent structural transformation into **CP-Hp-2** gradually upon spontaneous release of solvent molecules under ambient conditions. Upon the transformation, the network topology of the original structure remained, while periodicity of the framework was shrunk by 4.1 Å along the [010] direction corresponding to the shorter diagonal of the rhombic aperture and elongated by 1.6 Å along the [101] direction corresponding to the longer diagonal of the aperture (Table S1, Supporting Information). A host-guest ratio of **CP-Hp** and DCB changed from 1:4 to 1:2 upon the transformation (Figure S3, Supporting Information). The transformation from **CP-Hp-1** into **CP-Hp-2** changes the space group from $P2_1/c$ to $C2/m$ (Table S1, Supporting Information). This is because the propylene part

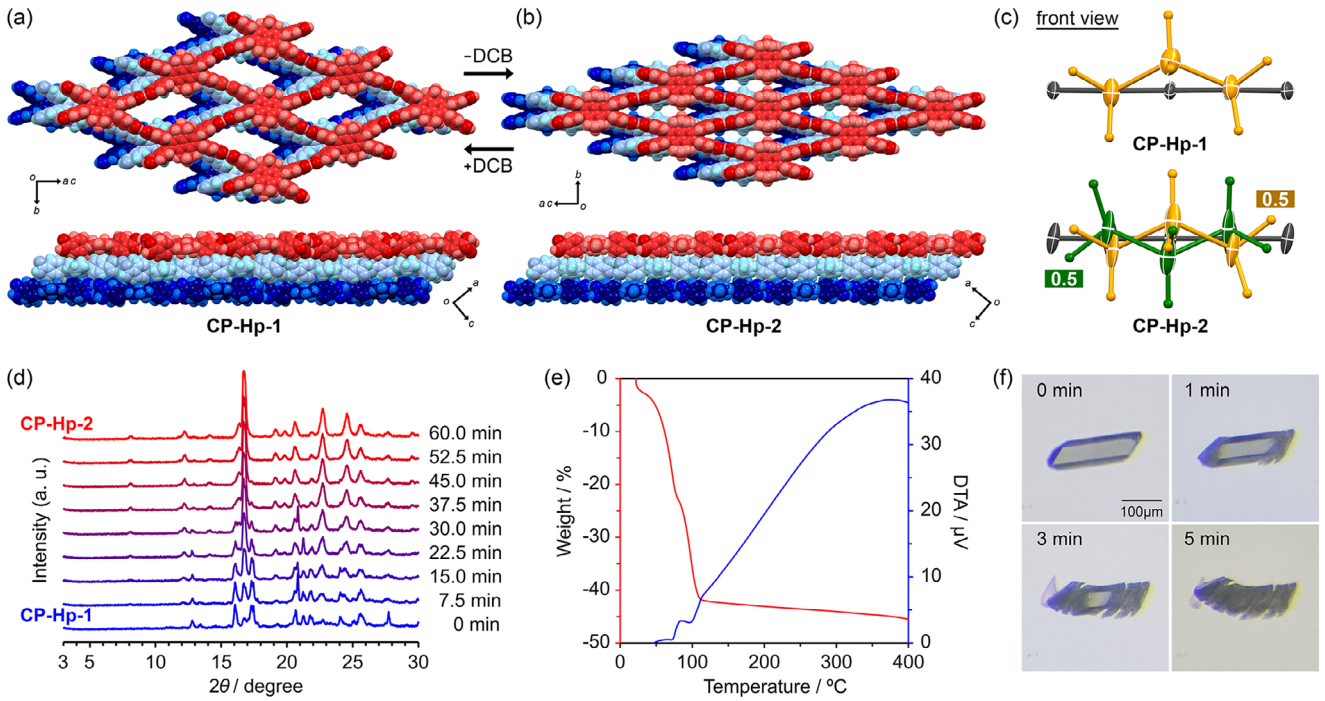

Figure 2. Structural transformation of **CP-Hp-1** to **CP-Hp-2**. Crystal structures of a) **CP-Hp-1** and b) **CP-Hp-2** revealed by SCXRD analysis, where molecules of included DCB are omitted. c) Propylene parts in the central hexahydropyrene cores in **CP-Hp-1** and **CP-Hp-2**. The part in **CP-Hp-2** was disordered into two conformations, colored yellow and green, with a 1:1 ratio. d) PXRD pattern changes from **CP-Hp-1** to **CP-Hp-2** in the bulk crystalline state. e) TG-DT curves. f) Morphological changes of a single crystal of **CP-Hp-1** after wiping off the bulk solvent from the surface of the crystal. The structure of **CP-Hp-1** was drawn using crystal data (CCDC No. 2206158) previously reported.[24]

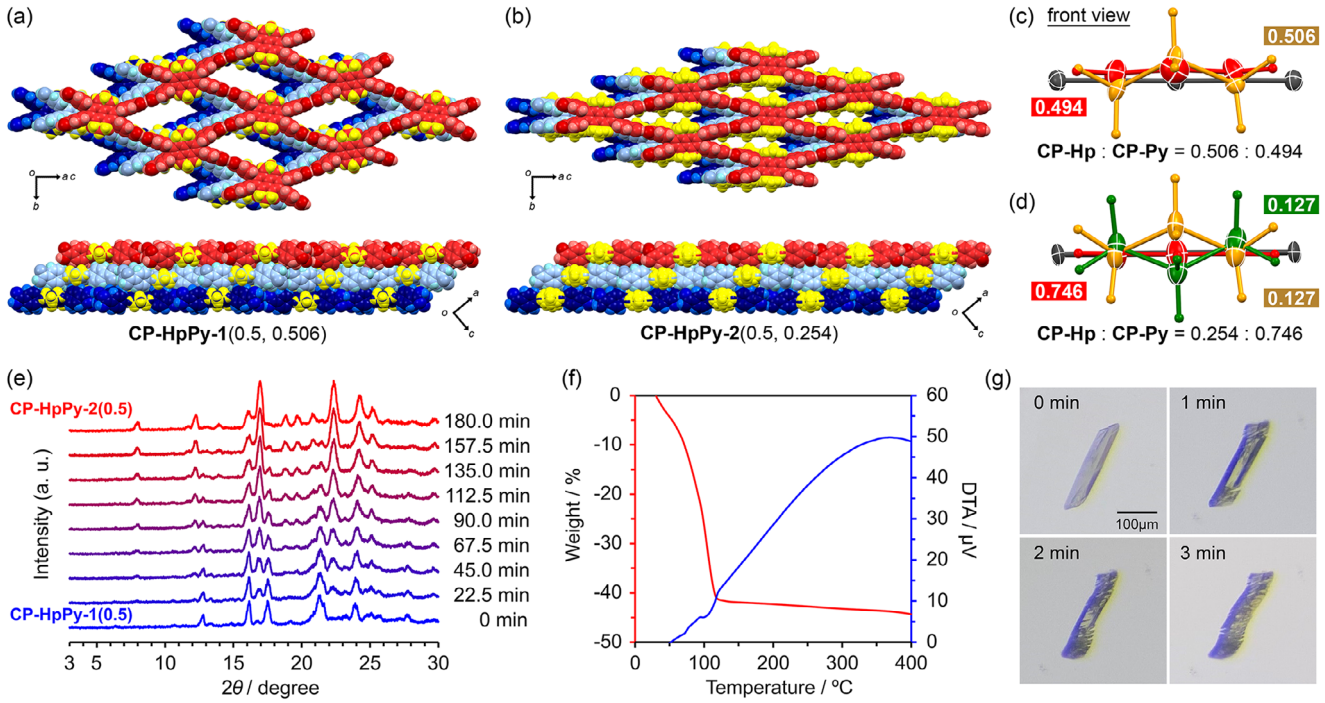

Figure 3. Structural transformation of **CP-HpPy-1**(0.5) to **CP-HpPy-2**(0.5). Representative crystal structures of a) **CP-HpPy-1**(0.5, 0.506) and b) **CP-HpPy-2**(0.5, 0.254) revealed by SCXRD analysis, where molecules of included DCB are omitted. Disordered structure of the hydropyrene (yellow and green) and pyrene (red) core in c) **CP-HpPy-1**(0.5, 0.506) and d) **CP-HpPy-2**(0.5, 0.254). e) PXRD pattern changes from **CP-HpPy-1**(0.5) to **CP-HpPy-2**(0.5), f) TG and DT curves, (g) Morphological changes of a single crystal of **CP-HpPy-1**(0.5) after wiping off bulk solvent from the surface of the crystal. The structure of **CP-Hp-1**(0.5, 0.506) was drawn using crystal data (CCDC No. 2206160) previously reported.[24]

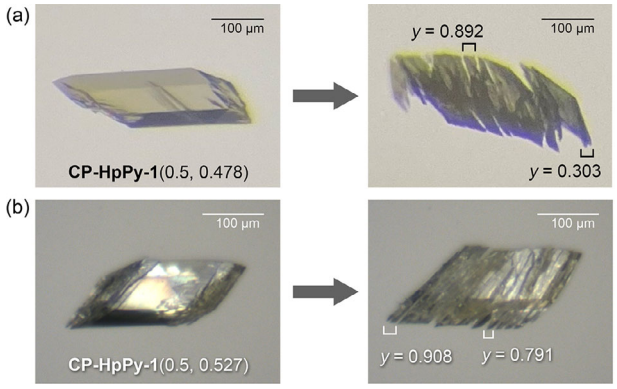

Figure 4. Crystalline morphology and composition ratio of a) **CP-HpPy-1**(0.5, 0.478) and b) **CP-HpPy-1**(0.5, 0.527) before and after the transformation into **CP-HpPy-2**. The ratio of **CP-HpPy-1** was determined by SXRD analysis on the whole crystal, while that of **CP-HpPy-2** was on a platelet fragment picked from the cracked crystal.

of the hydropyrene core is disordered into two positions with the up and down conformations related to the σ_h plane on the core (Figure 2c). This symmetrical change of **CP-Hp-1** is not observed for **CP-Py-1**, which keeps the space group of $P2_1/c$ upon the transformation (Table S2, Supporting Information). Dihedral angles of the peripheral phenylene groups against the cores and shapes of the apertures of **CP-Py-2** and **CP-Hp-2** also slightly differ from each other (Figure S4 and Table S5, Supporting Information).

Time-dependent powder X-ray diffraction (TD-PXRD) measurement showed that the diffraction peaks ascribable to **CP-Hp-1**, such as those at 2θ of 12.8°, 13.3°, 16.0°, and 17.3°, gradually disappeared, while new peaks ascribable to **CP-Hp-2**, such as those at 8.1°, 12.2°, 16.7°, and 22.7° appeared (Figure 2d). The rapid weight loss observed in the thermal gravimetric (TG) curve and endothermic peaks in the differential thermal (DT) curve support the structural transformation that occurs by the release of guest molecules (Figure 2e). The addition of a drop of **CP-Hp-2** quickly recovered the initial form **CP-Hp-1**, indicating the reversible transformation between these two crystalline forms (Figure S5, Supporting Information). When **CP-Hp-2** was further left under ambient conditions, the diffraction peaks ascribable to **CP-Hp-2** decayed and new peaks appeared at 8.7°, 13.8°, 17.4°, and 20.3°, indicating further transformation into the third form **CP-Hp-3** (Figure S6, Supporting Information), although the crystal structure could not be determined by SCXRD analysis due to the low single crystallinity.

Focusing on the morphology of a single crystal, a columnar crystal of **CP-Hp-1** started to get cracks from the edges after wiping off the bulk solvent on the surface (Figure 2f). For detailed morphological changes of single crystals, see Movie S1 (Supporting Information). Interestingly, the resultant platelet pieces retained single crystallinity, allowing us to reveal the crystal structure of **CP-Hp-2** by SCXRD as described above (Figure 2b).

2.2. Structural transformation of NS-HOF CP-HpPy-1

Mixtures of **CP-Hp** and **CP-Py** in various composition ratios were dissolved in a mixed solution of DMF and DCB and left at 100 °C to evaporate solvent slowly, giving crystals of NS-HOFs **CP-HpPy-1**(x, y), where x and y denote the molar fraction of **CP-Hp** in the initial solution and crystallographically-determined occupancy of **CP-Hp** in the resultant single crystal of **CP-HpPy-1**, respectively. The crystals whose y has not been determined are simply presented by **CP-HpPy-1**(x). NS-HOFs **CP-HpPy-1**(x) also underwent structural transformation into **CP-HpPy-2**(x) upon the spontaneous solvent release (**Figure 3**; Figures S8–S13, Supporting Information). The structural transformation between **CP-HpPy-1**(x) and **CP-HpPy-2**(x) was reversible (Figures S14–S16, Supporting Information), and we confirmed that multiple cycles of conversion between them were possible (Figure S17, Supporting Information). The crystal structures of **CP-HpPy-1**(x) and **CP-HpPy-2**(x) were solved using the disorder model of **CP-Hp** and **CP-Py**, and the composition ratio of each single crystal was capable of being determined by optimizing their occupancies.

Representative crystal structures of **CP-HpPy-1** and **CP-HyPy-2** are shown in Figure 3a,b, respectively. A single crystal of **CP-HpPy-1** was picked out from a crystallization batch with the mixing ratio of $x = 0.5$. SCXRD analysis revealed that the crystal exhibited a composition ratio of $y = 0.506$: the crystal is denoted as **CP-HpPy-1**(0.5, 0.506). The structure is basically the same as the monocomponent crystal except for the disordered core parts (Figure 3c). The crystal structure of **CP-HpPy-2**(0.5) exhibits a ***sql***-topological network sheet with narrow apertures (Figure 3b). The core moiety is composed of disordered pyrene and hydropyrene structures. Propylene parts of the hydropyrene core are further disordered into two parts, and therefore, the core is disordered into three parts (Figure 3d). Based on the refinement of the occupancies, the composition ratio of **CP-Hp** and **CP-Py** in the crystal of **CP-HpPy-2** is revealed to be 0.254:0.746 (Figure 2d). Therefore, the crystal is abbreviated as **CP-HpPy-2**(0.5, 0.254).

The structural change of bulk crystals of **CP-HpPy-1**(0.5) into **CP-HpPy-2**(0.5) was monitored by a TD-PXRD measurement. The diffraction peaks ascribable to **CP-HpPy-1**, such as those at 2θ of 13.8°, 16.1°, 17.5°, and 21.3° were gradually replaced by peaks at 2θ of 8.0°, 12.2°, 17.0°, and 22.3° ascribable to **CP-HpPy-2** (Figure 3e). TG and DT curves support the structural transformation that occurs by the release of guest molecules, as in the case of **CP-Hp-1** (Figure 3f). A rod-shaped single crystal of **CP-HpPy-1**(0.5) got cracks upon the transformation (Figure 3g) (For details, see Movies S1–S5, Supporting Information). The resultant platelet pieces retained single crystallinity and allowed us to determine their crystal structures and the composition ratio.

It should be mentioned that the ratio (y) was not matched between **CP-HpPy-1** and **CP-HpPy-2**, even when the SCXRD measurements were conducted on the same crystal, but before and after the transformation. This is because component distribution is not completely uniform like an ideal solid solution, although the distribution in the present system is relatively uniform compared to other systems.[26] The composition ratio of **CP-HpPy-1** determined by SCXRD analysis is an average value of the entire single crystal, while the ratio of **CP-HpPy-2** was for one of the cracked platelet fragments, which reflects the local structure of the original crystal. For example, the SCXRD analysis revealed that platelet pieces located at the different positions in the cracked crystal of **CP-HpPy-1**(0.5, 0.478) exhibit the y values of 0.892 and 0.303, as shown in **Figures** 4a and S18 (Supporting Information). Similarly, two platelet pieces picked from the cracked crystal of

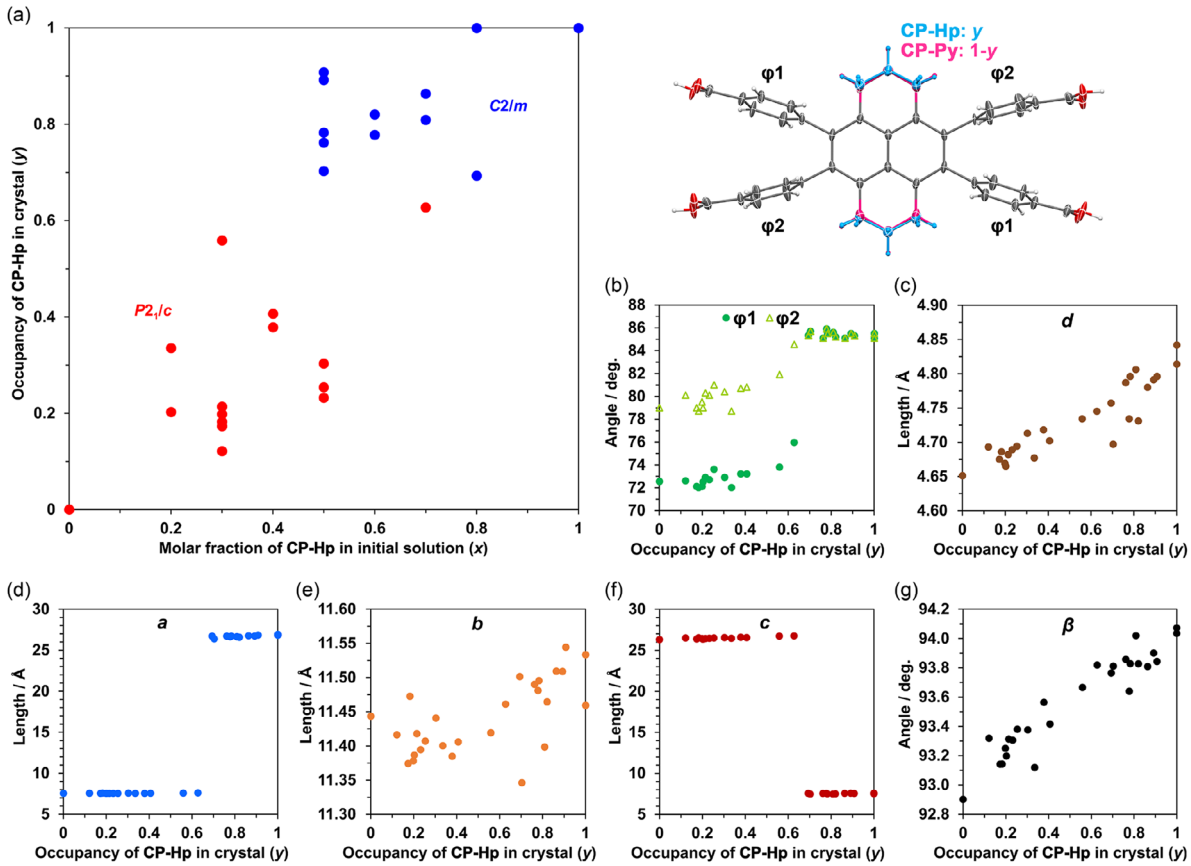

Figure 5. a) Composition in single-crystals of **CP-HpPy-2**(*x*, *y*), where x and y denote the molar fraction or occupancy of **CP-Hp** in the initial solution and the resultant single crystal, respectively. The crystals corresponding to the blue plots have the space group of *C*2/*m*, and the pink plots have that of $P2_1/c$. b) The dihedral angles $\varphi 1$ and $\varphi 2$ of the peripheral phenylene groups relative to the naphthalene for **CP-HpPy-2**(x, y). c) Intermolecular distance d for **CP-HpPy-2** with various y values. Crystallographic parameters for **CP-HpPy-2** with various y values: d) *a* axis, e) *b* axis, f) *c* axis, g) angle β.

CP-HpPy-1(0.5, 0.527) showed the *y* values of 0.908 and 0.791 (Figure 4b; Figure S19, Supporting Information).

To explore the structural details of **CP-HpPy-2** with different composition ratios, we prepared bulk crystals of **CP-HpPy-1**(*x*), where $x = 0.2$, 0.3, 0.4, 0.5 0.6, 0.7, and 0.8, by mixing **CP-Hp** and **CP-Py**. In total, 25 platelet pieces were corrected from the cracked crystals of **CP-HpPy-1**(*x*) and analyzed by SCXRD (Figures S20,S22; Table S4, Supporting Information). **Figure** 5a shows the relationship between the *x* and *y* values of **CP-HpPy-2**. The proportional relationship between *x* and *y* is considerably lower than that of **CP-HpPy-1**.[24] This is likely due to the manifestation of the inhomogeneous component distribution in localized areas of the crystal of **CP-HpPy-1**. Particularly, the *y* values at $x = 0.5$ are widely dispersed from 0.232 to 0.908. Platelet fragments corrected from a crystal of **CP-HpPy-1**(0.3, 0.272) and **CP-HpPy-1**(0.7, 0.715) were also analyzed by SCXRD to determine the composition ratio of the corresponding **CP-HpPy-2** crystals, resulting in the dispersed *y* values such as $y = 0.182$ and 0.559 (Figures S20 and S21, Supporting Information).

It was revealed that the space group of **CP-HpPy-2** depends on the *y* value. **CP-HpPy-1**(*x*, *y*) changes to **CP-HpPy-2**(*x*, *y*) with the space group of $P2_1/c$ when the **CP-Py** composition is higher than 0.35 (i.e., $y < 0.65$) and to that with the space group of *C*2/*m* when the **CP-Hp** composition is higher than 0.65 (Figure 5a; Table S4, Supporting Information). The change of space group is provided by changes in symmetry related to the dihedral angles ($\varphi 1$ and $\varphi 2$) of the peripheral phenylene groups against the central naphthalene ring: for the crystals with $y < 0.65$, $\varphi 1$ and $\varphi 2$ are different at ≈73° and 80°, respectively, whereas for those with $y > 0.65$, $\varphi 1$ and $\varphi 2$ are equal at ≈86° (Figure 5b; Figures S23 and S24, Supporting Information). The changes in the dihedral angles may be caused by the nonplanar conformation of the hydropyrene core. When the ratio of **CP-Hp** increases, the averaged intermolecular distance (*d*) between stacked molecules also increases, making the dihedral angle nearly perpendicular. In fact, distance *d* increases from 4.65 Å to 4.84 Å as *y* value increases from 0 to 1 (Figure 5c), and both dihedral angles $\varphi 1$ and $\varphi 2$ also increase up to 86°, resulting in two types of frameworks with different symmetries depending on the *y* value. **CP-HpPy-2**(*x*, *y*) ($y < 0.65$) has distorted rhombic apertures similar to **CP-Py-2**, while **CP-HpPy-2**(*x*, *y*) ($y > 0.65$) has rhombic ones similar to **CP-Hp-2** (Figures S25 and S4, Supporting Information). The cell parameters of **CP-HpPy-2**(*x*, *y*) also change as the *y* value increases from 0 to 1. The lengths of the *a* and *c* axes of the unit cell change discontinuously around $y = 0.65$ from 7.55 to 26.7 Å and from 26.7 to 7.55 Å, respectively, due to the changes of space groups (Figure 5d,f). The length of the *b* axis of the unit cell has no clear

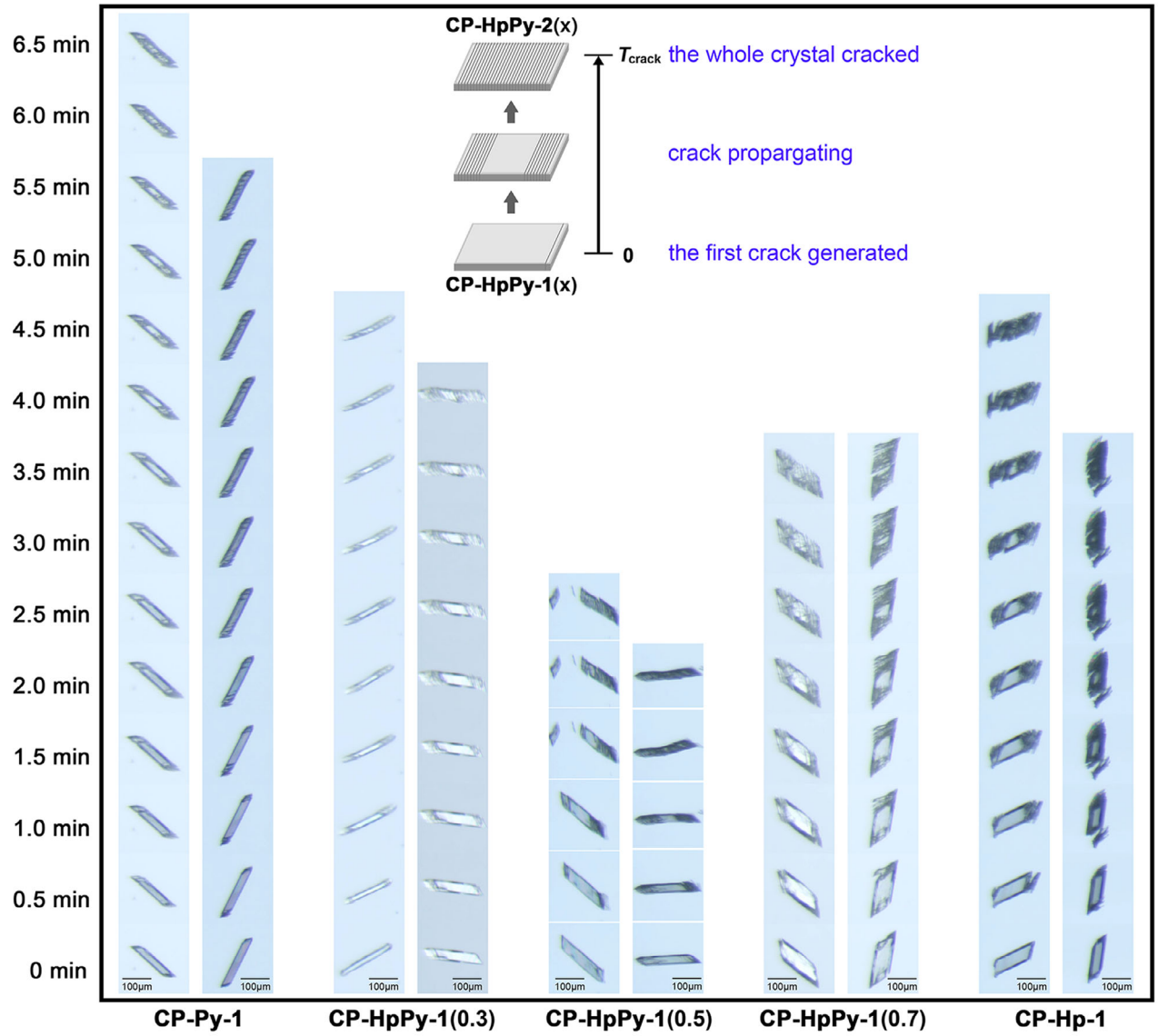

Figure 6. Morphology changes of two representative single crystals for each of **CP-Py-1**, **CP-HpPy-1**(0.3), **CP-HpPy-1**(0.5), **CP-HpPy-1**(0.7), and **CP-Hp-1**. (Inset) Schematic representation of the crack propagation, where Tcrack is defined as the time from when the first crack is generated until the cracks cover the entire crystal.

correlation with the γ value (Figure 5e). The β angle of the unit cell increases continuously from 92.9° to 94.1° (Figure 5g).

2.3. Structural Transformation Speed Depending on the Composition Ratio

As described above, the single crystals get cracks gradually from the edges with the structural transformation triggered by the release of guest molecules.

The cracks are nearly parallel to the (1 0 −4) plane, which corresponds to the H-bonded 2D layers (Figure S7, Supporting Information). Therefore, the cracking part shows that the transformation is occurring there, and the cracking speed spreading throughout the entire crystal can be regarded as the structural transformation speed in a single crystal.

We investigated the composition ratio dependence of the structural transformation of the NS-HOF **CP-HpPy-1**. The crystals picked up from batches were washed with DCB, and the bulk solvent on the crystal surface was whipped off. Then, we recorded the time course of the morphological changes and measured the time from when the first crack was generated until the cracks covered the entire crystal. The time is denoted by T_{crack}. Totally, 82 single crystals of **CP-HpPy-1**(x) with $x = 0$, 0.3, 0.5, 0.7, or 1 were subjected to the measurements. In **Figure 6**, the time courses of morphological changes in two representative crystals for each of **CP-Py-1** ($x = 0$), **CP-HpPy-1**(x) ($x = 0.3$, 0.5, 0.7), and **CP-Hp-1** ($x = 1$) are shown. A crystal of **CP-Py-1**, represented by $x = 0$,

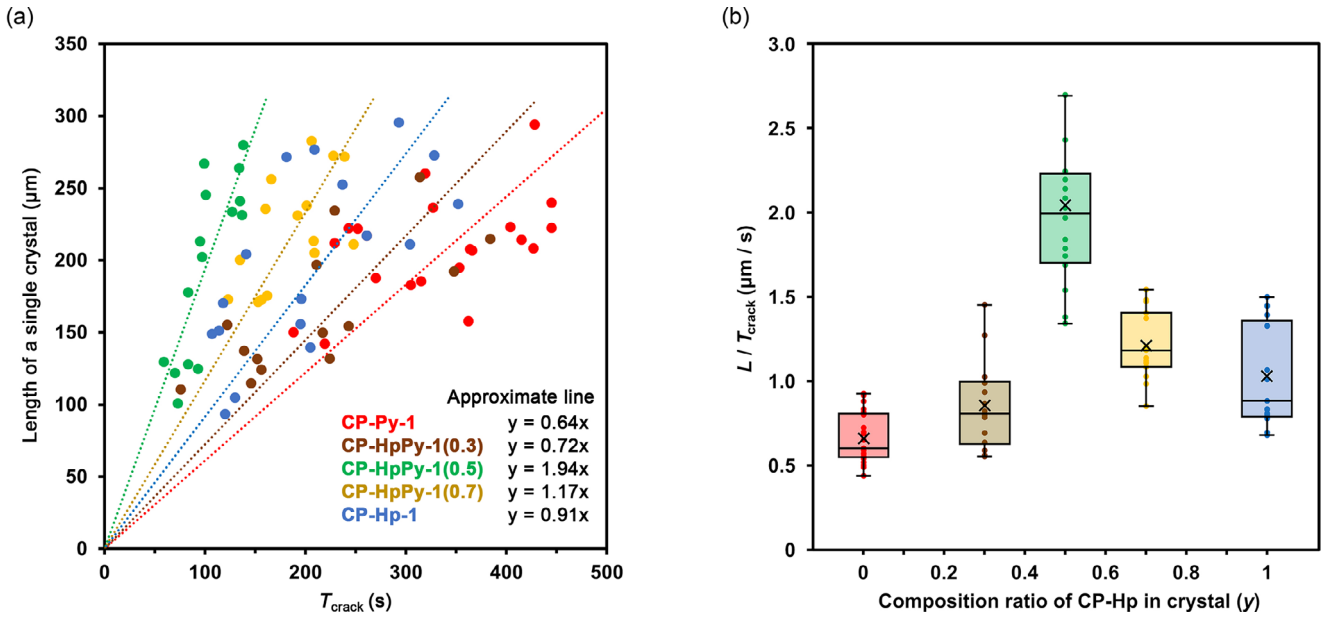

Figure 7. a) Relationship between the time taken for the entire single crystals to crack (T_{crack}) and their length. b) Relationship between the transformation speed ($S = L / T_{crack}$) and the composition ratio of **CP-Hp** in the crystal (y).

showed T_{crack} of ca. 6.5 min, while a crystal of **CP-Hp-1**, represented by $x = 1$, showed T_{crack} of ca. 4 min, which is shorter than that of **CP-Py-1**. Moreover, it is remarkable that the T_{crack} value of NS-HOFs **CP-HpPy-1**(x) (x = 0.3, 0.5, 0.7) changes in a non-linear way as x value increases, instead of a proportional change between the values of **CP-Py-1** and **CP-Hp-1**. **CP-HpPy-1**(0.5) exhibits the smallest value, although the length (L) of single crystals along the long axis is nearly identical at ≈200 μm. Additionally, a crystal of **CP-Hp-1** is divided into smaller pieces than **CP-Py-1** upon the transformation. Crystals of **CP-HpPy-1**(x) tended to be divided into smaller pieces as the x value increased. These are probably caused by the disorder of the hydropyrene core, as well as the large changes in the dihedral angle of the peripheral phenylene groups: the angle changes by up to 10.6° in the transformation from **CP-Py-1** to **CP-Py-2**, while 12.3° from **CP-Hp-1** to **CP-Hp-2** (Table S5, Supporting Information).

We also measured the ratio of cracked parts in a single crystal every 5 s to reveal how the heterogeneity in a crystal affects crack propagation (Figure S26a, Supporting Information). In **CP-Py-1**, the ratio increased discretely, whereas in **CP-Hp-1**, it did continuously. This is because a crystal of **CP-Py-1** divides into larger pieces than that of **CP-Hp-1** (Figures S26b,c, S27, and S31, Supporting Information). In **CP-HpPy-1(*x*)** (x = 0.3, 0.5, 0.7), both continuous and discrete increases were observed in the plots (Figure S26d–f, Figures S28–S30, Supporting Information), indicating that some parts in a crystal are divided into large pieces, while others are done into small ones. These results are expected to be due to the heterogeneity of distribution in a crystal.

To clarify the relationship between the transformation speed and the composition ratio, T_{crack} and L for the examined single crystals are plotted as shown in **Figure 7a**. L and T_{crack} are roughly proportional to each other. The slope represents the average cracking speed (S). The value of S changes depending on the composition ratios in the single crystals, where we assume that the value of x can be treated as y because the composition ratio (y) of NS-HOF single crystals has a moderately good proportional correlation with the mixing ratio (x), as we revealed.[24]

Figure 7b shows a statistical summary of cracking speed ($S = L/T_{crack}$) for each of **CP-Hp-1**, **CP-Py-1**, and **CP-HpPy-1**(x) (x = 0.3, 0.5, 0.7), respectively. For each composition ratio, the median and the average values of S were approximately the same. The graph reasonably indicates that the cracking speed increases in the order **CP-Py-1** < **CP-HpPy-1**(0.3) < **CP-Hp-1** < **CP-HpPy-1**(0.7) < **CP-HpPy-1**(0.5). Importantly, S of **CP-HpPy-1**(x) (x = 0.3, 0.5, 0.7) does not vary linearly between the values of **CP-Py-1** and **CP-Hp-1**, while it does non-linearly as the composition ratio changes. The maximum value of S was observed for **CP-HpPy-1**(0.5).

The observed transformation speed can be explained as follows. The destabilization of the framework caused by the mixing of the two components makes the transformation speed faster. Comparison of **CP-Py-1** and **CP-Hp-1** structures shows that the dihedral angles relative to the naphthalene rings, the framework periodicity, and the guest molecules' positions are slightly different (Figure S1, Tables S1 and S2, Supporting Information). In addition, as revealed in our previous study, **CP-HpPy-1** is the kinetically formed crystal with heterogeneous distribution. These facts support that **CP-HpPy-1** has more structural defects than mono-component crystals and undergoes structural transformation at a faster speed.

3. Conclusion

In this paper, we report the structural transformation behavior of mono-component HOF **CP-Hp-1** and non-stoichiometric cocrystalline HOF **CP-HpPy-1**. These HOFs were revealed to change into the second crystalline form by the release of guest molecules. **CP-Hp-1** has an identical crystal structure to **CP-Py-1**, but

CP-Hp-2, the second crystalline form, has a different structure from **CP-Py-2**. **CP-HpPy-1** changes into two different structures depending on the main component. Furthermore, the transformation speed changes non-linearly with increasing the composition ratio of **CP-Hp** in the framework: **CP-HpPy-1**(0.5) has the fastest transformation speed. These results are the first examples of modulating the transformation behavior of the porous framework depending on the composition ratio and provide important insights into the development of flexible non-stoichiometric cocrystalline frameworks.

4. Experimental Section

Determination of the Transformation Speed: Wet single crystals of HOF **CP-Hp-1**, **CP-Py-1,** and **CP-HpPy-1** were placed on a glass plate, and the bulk solvent on the surfaces of the single crystals was carefully wiped off using thin fibers of tissue paper. The single crystals were left under ambient conditions, starting crack propagation corresponding to the structural transformation from **CP-Hp-1**, **CP-Py-1,** and **CP-HpPy-1** to **CP-Hp-2**, **CP-Py-2,** and **CP-HpPy-2**, respectively, which was recorded on video. The transformation speed (*S*) was calculated by dividing the crystal length (*L*) along the long axis by the time it took for crack propagation (T_{crack}).

Supporting Information

Supporting Information is available from the Wiley Online Library or from the author.

Acknowledgements

This work was supported by KAKENHI (JP23H04029, JP24K01468, JP25H01672, JP25H02042) from JSPS and MEXT Japan. T.H. thanks the financial support by Grant-in-Aid for JSPS Research Fellow (JP24KJ1655). I.H. thanks Hoansha Foundation. The authors thank the Cybermedia Center, The University of Osaka, for the use of the Super-computer for Quest to Unsolved Interdisciplinary Datascience (SQUID). The authors acknowledge Ms. R. Miyake at The University of Osaka for HR-MS analysis.

Conflict of Interest

The authors declare no conflict of interest.

Data Availability Statement

Deposition numbers 2464130 (for **CP-Hp-2**), 2464131 (for **CP-HpPy-2**(0.5, 0.254)), and 2464132 (for **CP-HpPy-2**(0.5, 0.703)) contain the supplementary crystallographic data for this paper. These data are provided free of charge by the joint Cambridge Crystallographic Data Centre and Fachinformationszentrum Karlsruhe Access Structures service.

Keywords

carboxylic acid, flexible framework, hydrogen bond, mixed crystal

Received: July 22, 2025
Revised: October 8, 2025
Published online:

[1] H. Furukawa, U. Müller, O. M. Yaghi, *Angew. Chem., Int. Ed.* **2015**, *54*, 3417.
[2] S. P. Teong, Y. Zhang, *ChemNanoMat* **2023**, *9*, 202300263.
[3] S. J. Lee, S. G. Telfer, *Angew. Chem., Int. Ed.* **2023**, *62*, 202306341.
[4] V. Guillerm, D. Kim, J. F. Eubank, R. Luebke, X. Liu, K. Adil, M. S. Lah, M. Eddaoudi, *Chem. Soc. Rev.* **2014**, *43*, 6141.
[5] S. Yuan, L. Feng, K. Wang, J. Pang, M. Bosch, C. Lollar, Y. Sun, J. Qin, X. Yang, P. Zhang, Q. Wang, L. Zou, Y. Zhang, L. Zhang, Y. Fang, J. Li, H.-C. Zhou, *Adv. Mater.* **2018**, *30*, 1704303.
[6] J.-R. Li, J. Sculley, H.-C. Zhou, *Chem. Rev.* **2012**, *112*, 869.
[7] H. Deng, C. J. Doonan, H. Furukawa, R. B. Ferreira, J. Towne, C. B. Knobler, B. Wang, O. M. Yaghi, *Science* **2010**, *327*, 846.
[8] K. Geng, T. He, R. Liu, S. Dalapati, K. T. Tan, Z. Li, S. Tao, Y. Gong, Q. Jiang, D. Jiang, *Chem. Rev.* **2020**, *120*, 8814.
[9] S. Ge, K. Wei, W. Peng, R. Huang, E. Akinlabi, H. Xia, M. W. Shahzad, X. Zhang, B. B. Xu, J. Jiang, *Chem. Soc. Rev.* **2024**, *53*, 11259.
[10] S. Kandambeth, K. Dey, R. Banerjee, *J. Am. Chem. Soc.* **2019**, *141*, 1807.
[11] R. L. Li, A. Yang, N. C. Flanders, M. T. Yeung, D. T. Sheppard, W. R. Dichtel, *J. Am. Chem. Soc.* **2021**, *143*, 7081.
[12] M. Wang, T. Zeng, Y. Yu, X. Wang, Y. Zhao, H. Xi, Y.-B. Zhang, *J. Am. Chem. Soc.* **2024**, *146*, 1035.
[13] D. Ren, H.-L. Xia, K. Zhou, S. Wu, X.-Y. Liu, X. Wang, J. Li, *Angew. Chem., Int. Ed.* **2021**, *133*, 25252.
[14] J. Perego, C. X. Bezuidenhout, I. Villa, F. Cova, R. Crapanzano, I. Frank, F. Pagano, N. Kratochwill, E. Auffray, S. Bracco, A. Vedda, C. Dujardin, P. E. Sozzani, F. Meinardi, A. Comotti, A. Monguzzi, *Nat. Commun.* **2022**, *13*, 3504.
[15] W. J. Newsome, S. Ayad, J. Cordova, E. W. Reinheimer, A. D. Campiglia, J. K. Harper, K. Hanson, F. J. Uribe-Romo, *J. Am. Chem. Soc.* **2019**, *141*, 11298.
[16] K. C. Park, C. Seo, G. Gupta, J. Kim, C. Y. Lee, E. E. Transfer, *ACS Appl. Mater. Interfaces* **2017**, *9*, 38670.
[17] J. Y. Choi, M. Wang, B. Check, M. Stodolka, K. Tayman, S. Sharma, J. Park, *Small* **2023**, *19*, 2206988.
[18] N. Huang, L. Zhai, D. E. Coupry, M. A. Addicoat, K. Okushita, K. Nishimura, T. Heine, D. Jiang, *Nat. Commun.* **2016**, *7*, 12325.
[19] B. Wang, R.-B. Lin, Z. Zhang, S. Xiang, B. Chen, *J. Am. Chem. Soc.* **2020**, *142*, 14399.
[20] X. Song, Y. Wang, C. Wang, D. Wang, G. Zhuang, K. O. Kirlikovali, P. Li, O. K. Farha, *J. Am. Chem. Soc.* **2022**, *144*, 10663.
[21] I. Hisaki, C. Xin, K. Takahashi, T. Nakamura, *Angew. Chem., Int. Ed.* **2019**, *131*, 11278.
[22] T. Miyano, I. Hisaki, N. Tohnai, *Chem. Lett.* **2017**, *46*, 225.
[23] Q. Chen, T. Zhang, X. Chen, M. Liang, H. Zhao, P. Yuan, Y. Han, C.-P. Li, J. Hao, P. Xue, *ACS Appl. Mater. Interfaces* **2022**, *14*, 24509.
[24] T. Hashimoto, R. Oketani, M. Nobuoka, S. Seki, I. Hisaki, *Angew. Chem., Int. Ed.* **2023**, *135*, 202215836.
[25] X. Y. Gao, Y. Wang, E. Wu, C. Wang, B. Li, Y. Zhou, B. Chen, P. Li, *Angew. Chem., Int. Ed.* **2023**, *62*, 202312393.
[26] T. Hashimoto, M. de la Hoz Tomás, R. Oketani, B. Cohen, M. Naruoka, N. Tohnai, A. Douhal, I. Hisaki, S. Crystalline, *Angew. Chem., Int. Ed.* **2025**, *64*, 202419992.
[27] T. Hashimoto, R. Oketani, A. Inoue, K. Okubo, K. Oka, N. Tohnai, K. Kamiya, S. Nakanishi, I. Hisaki, *Chem. Commun.* **2023**, *4*, 7224.
[28] S. Kitagawa, K. Uemura, *Chem. Soc. Rev.* **2005**, *34*, 109.
[29] S. Horike, S. Shimomura, S. Kitagawa, *Nat. Chem.* **2009**, *1*, 695.
[30] S. Seth, S. Jhulki, *Mater. Horiz.* **2021**, *8*, 700.

[31] J. Li, B. Chen, *Chem. Sci.* **2024**, *15*, 9874.
[32] H. Wang, B. Li, H. Wu, T.-L. Hu, Z. Yao, W. Zhou, S. Xiang, B. Chen, *J. Am. Chem. Soc.* **2015**, *137*, 9963.
[33] Q. Zhu, L. Wei, C. Zhao, H. Qu, B. Liu, T. Fellowes, S. Yang, A. Longcake, M. J. Hall, M. R. Probert, Y. Zhao, A. I. Cooper, M. A. Little, *J. Am. Chem. Soc.* **2023**, *145*, 23352.
[34] P. Cui, E. Svensson Grape, P. R. Spackman, Y. Wu, R. Clowes, G. M. Day, A. K. Inge, M. A. Little, A. I. Cooper, *J. Am. Chem. Soc.* **2020**, *142*, 12743.
[35] A. Pedrini, D. Marchetti, R. Pinalli, C. Massera, *ChemPlusChem* **2023**, *88*, 202300383.
[36] Q. Huang, W. Li, Z. Mao, L. Qu, Y. Li, H. Zhang, T. Yu, Z. Yang, J. Zhao, Y. Zhang, M. P. Aldred, Z. Chi, *Nat. Commun.* **2019**, *10*, 3074.
[37] L. Gong, Y. Ye, Y. Liu, Y. Li, Z. Bao, S. Xiang, Z. Zhang, B. Chen, *ACS Appl. Mater. Interfaces* **2022**, *14*, 19623.
[38] C. Jiang, J.-X. Wang, D. Liu, E. Wu, X.-W. Gu, X. Zhang, B. Li, B. Chen, G. Qian, *Angew. Chem., Int. Ed.* **2024**, *63*, 202404734.
[39] H. Kubo, S. Konishi, R. Oketani, T. Hayashi, I. Hisaki, *Chem. – Eur. J.* **2024**, *30*, 202401645.
[40] H. Kubo, R. Oketani, I. Hisaki, *Angew. Chem., Int. Ed.* **2025**, *54*, 202510977.
[41] H. Tsuji, I. Hisaki, *Chem. Eur. J. in press* 02303.